Atmospheric Environment 102 (2015) 331–343

Contents lists available at ScienceDirect

Atmospheric Environment

journal homepage: www.elsevier.com/locate/atmosenv

Ship-based MAX-DOAS measurements of tropospheric NO_2 and SO_2 in the South China and Sulu Sea

S.F. Schreier [a,*], E. Peters [a], A. Richter [a], J. Lampel [b], F. Wittrock [a], J.P. Burrows [a]

[a] Institute of Environmental Physics, University of Bremen, Germany
[b] Institute for Environmental Physics, University of Heidelberg, Germany

HIGHLIGHTS

- A profile retrieval approach to derive tropospheric NO_2 vertical columns is applied.
- The simple geometric approximation using 15° measurements can also be used.
- Time series of NO_2 and SO_2 are in good agreement in a busy shipping lane.

ARTICLE INFO

Article history:
Received 13 June 2014
Received in revised form
5 December 2014
Accepted 8 December 2014
Available online 8 December 2014

Keywords:
Ship-based MAX-DOAS measurements
Tropospheric NO_2
Geometric approximation
Profile retrieval
Tropospheric SO_2
Shipping emissions

ABSTRACT

In November 2011, ship-based Multi-Axis Differential Optical Absorption Spectroscopy (MAX-DOAS) measurements were performed within the SHIVA campaign on board RV Sonne in the South China and Sulu Sea. Spectral measurements for a total of eleven days could be used to retrieve tropospheric slant column densities (SCDs) of nitrogen dioxide (NO_2) and sulfur dioxide (SO_2) in the marine environment. The NO_2 fit was performed following recommendations developed during the CINDI campaign and adapted for the ship-based measurements. We found that the inclusion of a cross section for liquid water and an empirical correction spectrum accounting for the effects of liquid water and vibrational Raman scattering (VRS) slightly improved the NO_2 fit quality, especially at lower elevation angles and for lower NO_2 levels. The conversion of SCDs into tropospheric NO_2 vertical columns (TVC NO_2) has been achieved using both a simple geometric approach and the Bremian advanced MAX-DOAS Retrieval Algorithm (BREAM), which is based on the optimal estimation method and accounts for atmospheric radiative transfer. We found good agreement between the geometric approach using the 15° measurements and BREAM, revealing that measurements at 15° elevation angle can be used for retrieving TVC NO_2 in tropical marine environments when SZA is smaller than 75°. As expected, the values of TVC NO_2 were generally low ($<0.5 \times 10^{15}$ molec cm^{-2}) when no sources of NO_x were in proximity to the RV Sonne. However, we found increased values of TVC NO_2 ($>2 \times 10^{15}$ molec cm^{-2}) in the morning when the RV Sonne was heading along the coast of Borneo. This is in good agreement with satellite measurements. The results of the profile retrieval show that the boundary layer values of NO_2 are <30 pptv in the open and clean tropical marine environment. Interestingly, we also found elevated tropospheric SO_2 amounts for measurements taken in a busy shipping lane, consistent with the time series of tropospheric NO_2.

1. Introduction

Nitrogen oxides ($NO_x = NO + NO_2$) are well known and significant pollutants in the troposphere. Nitric oxide (NO) in the atmosphere is readily converted into the more harmful nitrogen dioxide (NO_2) by reaction with ozone (O_3). The reaction of NO_2 with the hydroxyl radical (OH) to form nitric acid (HNO_3) is the major loss process of NO_x during daytime. Loss processes at night are related to the formation of nitrate ion (NO_3) and dinitrogen pentoxide (N_2O_5) and the subsequent heterogeneous reactions of N_2O_5 at the surface and on aerosols. The main sources of NO_x are attributed to high-temperature combustion processes (e.g. fossil fuel burning, accidental and intentional biomass burning), soil microbial activity, and lightning (Lee et al., 1997).

* Corresponding author. Institute of Environmental Physics, University of Bremen, Otto-Hahn-Allee 1, D-28359 Bremen, Germany.
E-mail address: schreier@iup.physik.uni-bremen.de (S.F. Schreier).

http://dx.doi.org/10.1016/j.atmosenv.2014.12.015

Sulfur dioxide (SO_2) is a main constituent in the tropospheric sulfur cycle. Besides the natural emissions of dimethylsulfide (DMS), the anthropogenic emissions of SO_2 are quantitatively the most important emissions in the sulfur cycle (Berglen et al., 2004).

The amounts and distributions of NO_2 and SO_2 can be retrieved from active and passive remote sensing techniques in the ultraviolet (UV) and visible regions of the electromagnetic spectrum (e.g. Brewer et al., 1973). The Differential Optical Absorption Spectroscopy (DOAS) method (Perner and Platt, 1979), which is selected for the detection of NO_2 and SO_2 in this study, is a widely used technique in the UV/visible and was initially applied to the detection of tropospheric trace gases by active remote sensing using artificial light sources. However, the DOAS method is also applicable for passive remote sensing using direct and scattered sunlight as light source (Platt and Stutz, 2008).

After successful application of the zenith scattered light DOAS method, which mainly yields stratospheric trace gas amounts (Noxon, 1975; Solomon et al., 1987; Richter et al., 1999; Wittrock et al., 2000), the development of Multi-Axis (MAX) DOAS allowed for the extension of the technique to tropospheric trace gases and aerosols by observing scattered sunlight at different viewing directions (Hönninger et al., 2004; Wagner et al., 2004; Wittrock et al., 2004).

Although MAX-DOAS is relatively simple to operate, the interpretation of the data requires detailed information about the radiation transport in the atmosphere, especially in terms of aerosol scattering (Mie scattering). For example, Wagner et al. (2004) developed a method for deriving atmospheric aerosol profiles by using MAX-DOAS measurements of the oxygen dimer (O_4) under clear sky conditions. They demonstrated that the O_4 measurements are sensitive to the aerosol extinction close to the ground and suggested the potential to retrieve aerosol profiles by the use of radiative transfer models such as SCIATRAN (Rozanov et al., 2005) and McArtim (Deutschmann et al., 2011).

Ship-based MAX-DOAS measurements of NO_2 amounts have so far been focused on both remote and coastal marine environments in the Indian and Pacific Ocean to obtain boundary layer background conditions. Peters et al. (2012) reported NO_2 background conditions <50 pptv in the remote Western Pacific boundary layer, with tropospheric NO_2 columns rarely exceeding the detection limit of the instrument. Higher values of up to 200 pptv were estimated from MAX-DOAS observations on board the Japanese research vessel Kaiyo in the western Pacific and Indian Ocean boundary layer (Takashima et al., 2012), presumably being influenced by anthropogenic sources. However, during the NASA Pacific Exploratory Mission (PEM) Tropics B field experiment, aircraft in-situ measurements of NO_2 over the clean Pacific yielded values <10 pptv in the boundary layer (Browell et al., 2001). Consequently, the detection limit of the MAX-DOAS instrument (30–50 pptv) may be too large for actual measurements of NO_2 background values in the boundary layer. Nevertheless, the MAX-DOAS technique has an important benefit in retrieving tropospheric profile information of trace gases (see Sect. 4.4). While the focus of these previous studies was on NO_2 amounts, SO_2 has received much less attention. However, SO_2 emissions in the open sea are high because of the high sulfur contents in heavy fuels often used by ships in international waters (Endresen et al., 2005).

The Southeast Asian region experiences rapid environmental changes with some of the highest rates of deforestation in humid tropical forests as observed within the last two decades (Achard et al., 2002; Miettinen et al., 2011). Large areas of natural forest have been replaced by agricultural land, especially oil palm plantations. Miettinen et al. (2011) estimated the loss of the total forest area in insular Southeast Asia to be in the order of 10% between 2000 and 2010 and emphasize the continuing deforestation in this region.

In recent years, there has been an increasing interest on studying the effect of land use changes on tropospheric chemistry in tropical regions. MacKenzie et al. (2011) observed tropospheric trace gases over a rainforest and an oil palm site on Borneo Island. The results show that NO_x mixing ratios over the oil palm plantation were higher by a factor of 1.5 resulting from nitrogen fertilizer application and on-site palm oil processing. Rising concentrations of NO_x and volatile organic compounds (VOCs) over these plantations have increased the concentrations of some photochemical pollutants and could eventually increase tropospheric O_3 levels due to further industrialization and economic development (Hewitt et al., 2009). In addition to land use changes, international shipping emissions in the South China Sea are strongly driven by the increasing Asian trade volume (De Ruyter De Wildt et al., 2012).

The purpose of this manuscript is to report on daytime tropospheric NO_2 vertical columns (TVC NO_2) and profiles as well as SO_2 slant columns measured by a ship-based MAX-DOAS instrument in the coastal and open waters of the South China and Sulu Sea in November 2011. TVC NO_2 is retrieved by the profile inversion method BREAM and compared to TVC NO_2 as obtained from a geometric approach and from satellite instruments.

The MAX-DOAS measurements have been performed as part of the SHIVA ship-based campaign, which is briefly introduced and described in Sect. 2. The MAX-DOAS instrument and the retrieval of tropospheric NO_2 columns and profiles are introduced in Sect. 3. The results of this study for NO_2 and SO_2 are presented in Sect. 4 and summarized in Sect. 5. The satellite-based instruments and data products as well as the HYbrid Single-Particle Lagrangian

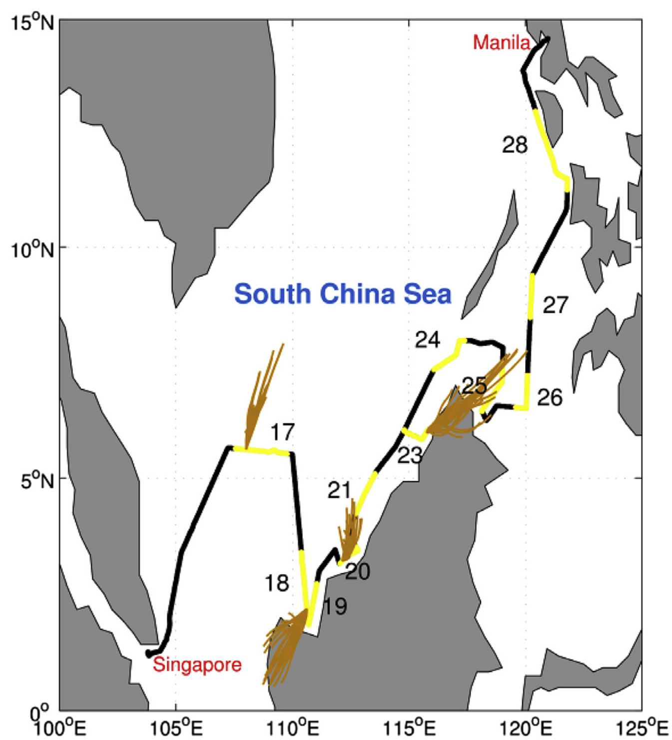

Fig. 1. Cruise track of the RV Sonne during SHIVA (black line), departing from Singapore on 15th November 2011 and arriving in Manila, Philippines on 29th November 2011. The sections of the cruise track highlighted in yellow indicate the distances traveled by the ship between the first and last daytime MAX-DOAS measurements presented in this study. The brown lines show ensembles of computed 12 h backward trajectories for selected case studies with TVC $NO_2 > 2 \times 10^{15}$ molec cm^{-2} (see Sect. 4.3). (For interpretation of the references to color in this figure legend, the reader is referred to the web version of this article.)

Integrated Trajectory (HYSPLIT) model, which is used for determining the origin of elevated NO_x levels in the study area can be found in the Appendix (electronic supplementary material).

2. Ship cruise within SHIVA

The aim of SHIVA (Stratospheric ozone: Halogen Impacts in a Varying Atmosphere) was to better predict the rate, timing and climate-sensitivity of ozone-layer recovery, and to identify potential risks from the recovery. For this purpose, several land-based, ship-based, aircraft-based, and space-based measurements in the insular region of Southeast Asia were combined with sophisticated numerical models (Pfeilsticker et al., in preparation).

The ship cruise was carried out with the German research vessel (RV) Sonne as a part of the SHIVA campaign between 15th November (departure: Singapore) and 29th November (arrival: Manila, Philippines) 2011 in the South China and Sulu Sea. The measurements made during the ship cruise aimed at (i) investigating the emissions of halogenated trace gases from coastal waters of the Western Pacific and upwelling waters, (ii) characterizing the marine biota causing these emissions of halogenated very short-lived substances, and (iii) studying the atmospheric transport and transformation of halogenated gases and their transport to the stratosphere (Pfeilsticker et al., in preparation). Indeed, the concentrations of NO_x and VOCs in insular Southeast Asia have risen due to land use changes and increased shipping emissions and thus, could affect the concentrations of ground-level ozone (Hewitt et al., 2009; De Ruyter De Wildt et al., 2012).

The IUP Bremen MAX-DOAS instrument was part of the RV Sonne instrumentation during SHIVA to measure atmospheric trace gases.

The entire ship track and daytime stages indicating the period between the first and last MAX-DOAS measurements are highlighted in Fig. 1. After installing and testing the instrument at the beginning of the campaign, continuous operation started in the morning of 17th November. Instrumental problems occurred in the middle of the campaign on 22nd November and therefore, no measurements are presented for this day. Overall, spectral measurements have been performed on eleven days during SHIVA, which provides a good basis for the analysis of NO_2 and SO_2 observations in the coastal and open waters of South China and Sulu Sea.

3. Instruments and data analysis

The DOAS technique is a widely-used remote sensing method to retrieve trace gases with narrow band absorption structures in the ultraviolet and visible part of the electromagnetic spectrum. Based on Lambert–Beer's law, this spectroscopic technique makes use of the absorption of electromagnetic radiation by matter. The DOAS principle can be applied to various ground-based, ship-based, aircraft-based, and satellite-based platforms (e.g. Platt and Stutz, 2008).

3.1. MAX-DOAS instrument and data retrieval

3.1.1. MAX-DOAS instrument

The MAX-DOAS instrument is an advancement of the zenith scattered light DOAS (e.g. Noxon, 1975) and Off-Axis DOAS (e.g. Sanders, 1993) that allows for measurements at different viewing directions (e.g. Hönninger et al., 2004).

Briefly, our MAX-DOAS instrument consists of a telescope unit, an optical fiber bundle, and a grating spectrometer. The telescope unit of the MAX-DOAS system collects scattered sunlight at selected viewing and azimuthal directions. Once the photons enter the entrance window of the telescope, they are focused by a lens to limit the field of view, before they move through an optical fiber bundle and reach a grating spectrometer equipped with a charge-coupled device (CCD) detector.

The telescope unit of the MAX-DOAS instrument assembled on board the RV Sonne includes a video camera (for weather and event detection) and was installed on a pan/tilt head. For measurements in the UV and visible range, grating spectrometers (Andor Shamrock 303i and Acton500, respectively) with a wavelength range of 305–373 and 392–563 nm and a spectral resolution of 0.4 and 0.8 nm, respectively, were used in combination with a CCD (Andor Newton DU940N and Roper Scientific Princeton NTE/CCD, respectively) with 512 × 2048 and 100 × 1340 pixels, respectively. Further characteristics of the MAX-DOAS system used within SHIVA can be found in Peters (2013).

During the recent CINDI (Cabauw Intercomparison campaign for Nitrogen Dioxide measuring Instruments) and TransBrom campaigns, the IUP-Bremen MAX-DOAS system was used to retrieved NO_2, formaldehyde (HCHO), and iodine monoxide (IO) (Roscoe et al., 2010; Peters et al., 2012; Piters et al., 2012; Großmann et al., 2013).

3.1.2. Set-up on the ship

During the SHIVA ship cruise, the azimuthal angle of the telescope unit was kept at 90° relative to the heading direction of the RV Sonne (Fig. 2) and elevation angles (α) of 1°, 2°, 3°, 4°, 5°, 6°, 7°, 8°, 9°, 10°, 15°, 30°, and 90° were included in the scanning sequence designed for the NO_2 retrieval. Each scanning sequence took about 15 min. In order to avoid the influence of twilight on the spectral measurements, the MAX-DOAS instrument was set to record off-axis spectra for solar zenith angles <85° (17th and 18th November) and <75° (19th to 28th November).

3.1.3. Data preparation and filtering

The ship's movements (heading, pitch, and roll) have been measured by the high accuracy (0.02°) Seatex MRU 5 instrumentation and downloaded from the ship's database at a time resolution of 50 ms after the campaign. The actual azimuthal direction and elevation angles of the scanning sequence have been corrected by the heading, pitch, and roll measurements afterward.

Due to the ship's movements in the sea, the elevation angles of the telescope, which are relative to the ship, are not the actual viewing directions. In order to overcome this effect, spectra were recorded with exposure times of 100 ms and ship's movements within this period were considered to be negligible. For each vertical scanning sequence, the individual 100 ms measurements were then corrected in terms of the roll angle and sorted according to the real viewing direction with a tolerance of ±0.5°. As this tolerance together with the instrument's field of view of ~1° could affect the quality of measurements at the 1° elevation angle (due to pointing into the water), the lowest viewing direction of the scanning sequence for the retrieval of tropospheric NO_2 was selected to be

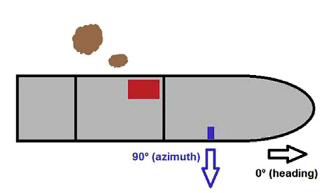

Fig. 2. Schematic illustration of the MAX-DOAS instrument set-up on board RV Sonne. The red rectangle indicates the ship's smoke stack and the blue rectangle depicts the position of the MAX-DOAS instrument, measuring in 90° azimuthal direction (blue arrow) relative to the ship's heading (black arrow). (For interpretation of the references to color in this figure legend, the reader is referred to the web version of this article.)

2°.

Finally, all of the individual measured spectra performed for each elevation angle of the scanning sequence (e.g. all 100 ms spectra obtained between 1.5° and 2.5° for $\alpha = 2°$) have been averaged. As a result, one average spectrum is achieved for each elevation angle of the individual scanning sequences.

Under unfavorable wind conditions, the ship's exhaust plume was potentially contaminating the measurements. As the instrument was installed in front of the ship's smoke stack (see Fig. 2), this was not a problem for most of the time when the ship was running at full speed. In order to exclude occasional influences of the ship's exhaust plume on the MAX-DOAS measurements, individual measurements taken under unfavorable wind directions (between 90° and 280°) have been discarded. The relative wind direction (blue dots) and the ship's speed (red line) are presented in Figs. 5a–7a for the individual days. In general, the ship's speed was higher than 20 km h^{-1} when it was running at full speed. In most such cases, the recorded relative wind direction was between 90° and 280°, which rules out any influence of the ship's smoke stack on the spectral measurements. It is apparent that unfavorable relative wind directions are more frequent when the ship slowed down. The bulk of data removed by data filtering occurred when the ship was slower than 5 km h^{-1}. However, the amount of spectral measurements after data filtering is still large enough for a reasonable analysis (>500 measured spectra per day on average). All spectral measurements within the two thresholds (90° and 280°, marked by the gray shaded area) are not included in the retrieval procedure, which is described in the following Sect. 3.1.4.

3.1.4. DOAS retrieval

3.1.4.1. Tropospheric NO_2 slant column densities. The filtered MAX-DOAS spectral measurements are analyzed using the DOAS technique applying a nonlinear least-squares fitting algorithm. Following recommendations developed during the CINDI and TransBrom campaigns (Piters et al., 2012; Peters et al., 2012), a fitting window between 425 and 490 nm has been selected. The high resolution absorption cross-sections of O_3 (Bogumil et al., 2003) at 223 K, NO_2 (Vandaele et al., 1996) at 298 K, O_4 (Greenblatt et al., 1990), H_2O (Rothmann et al., 2003) at 273 K, and a pseudo-cross section accounting for rotational Raman scattering as computed with SCIATRAN (Rozanov et al., 2005) have been included in the retrieval. In order to account for the influence of liquid water on the fit, we have added the liquid water absorption coefficient as measured in the laboratory by Pope and Fry (1997). Moreover, an empirical correction spectrum by Peters et al. (2014) accounting for the effects of liquid water and vibrational Raman scattering (VRS) has been included in the adapted NO_2 fit (see Table 1). For the retrieval of differential slant column densities (DSCDs), the zenith observation of the same measurement sequence was used as Fraunhofer reference spectrum (FRS). We note that for simplicity, we use the term SCD instead of DSCD throughout the manuscript.

As the RV Sonne left a dense shipping lane on the 17th November, we expect interesting insights into sulfur dioxide (SO_2) emissions from shipping. Therefore, we have also retrieved SO_2 from the MAX-DOAS UV measurements and will investigate the spatial distribution SO_2 columns and their relation to NO_2. However, the main focus of this study is on the tropospheric amounts and distributions of NO_2.

Table 1
Summary of the "standard" settings used for the visible spectra to produce NO_2 SCDs, including a cross section for liquid water and an empirical correction spectrum (italic) for the "adapted" fit (see Sect. 4.1). The set up for fitting in the UV to produce SO_2 SCDs is also listed (right).

	NO_2 settings	SO_2 settings
Fitting window [nm]	425–490	307.5–328
polynomial degree	5	3
O_3	Bogumil et al. (2003)	Gorshelev et al. (2014)
NO_2	Vandaele et al. (1996)	Vandaele et al. (1996)
O_4	Greenblatt et al. (1990)	–
H_2O	Rothman et al. (2003)[a]	–
SO_2	–	Bogumil et al. (2003)
Ring	SCIATRAN (VIS)	SCIATRAN (UV)
$H_2O_{liq.}$	*Pope and Fry (1997)*	–
empirical correction	*Peters et al. (2014)*	–

[a] But using HITRAN 2009.

3.1.4.2. Tropospheric SO_2 slant column densities. The SO_2 fit includes high resolution absorption cross-sections of O_3 (Gorshelev et al., 2014; Serdyuchenko et al., 2014) at 223 and 243 K, NO_2 (Vandaele et al., 1996) at 298 K, SO_2 (Bogumil et al., 2003) at 293 K, and a pseudo-cross section accounting for rotational Raman scattering as computed with SCIATRAN (Rozanov et al., 2005). The SO_2 fit was performed in the spectral window between 307.5 and 328 nm (see Table 1). As the UV spectrometer covers a wavelength range of 305–373 nm, the start wavelength was restricted. In order to cover the strongly structured SO_2 absorption spectrum around 300 nm (e.g. Richter, 2006), we have selected a wavelength range as close to the start wavelength as possible. The end wavelength of the interval was set to 328 nm because SO_2 fitting errors and RMS were small and reasonable values for the SO_2 SCDs were obtained, compared to other tested end wavelengths (not shown). In general, the SO_2 settings used in our study are comparable with those used in a recent study by Wang et al. (2014). They have retrieved SO_2 in the spectral range of 308–325 nm by including cross sections of SO_2, O_3, NO_2, and a synthetic ring spectrum. The SO_2 retrieval presented in Irie et al. (2011) is performed in a slightly smaller spectral window (310–320 nm) and includes an additional cross section for HCHO.

Due to some problems with the zenith SO_2 measurements (e.g. unexpected high values around noon causing a strong daily cycle), we have used the 30° measurements as FRS. As mentioned in Peters (2013), similar problems also occurred during TransBrom in the tropics at small SZAs for NO_2 and HCHO. One possible explanation could be that direct sunlight entering the system around noon in spite of light baffles leads to saturation effects on the CCD.

3.1.5. Conversion to tropospheric NO_2 vertical columns

In this study, the conversion of SCDs into TVCs is based on two different approaches:

The first approach uses the geometrical approximation by simply estimating a tropospheric air mass factor (AMF) via the $1/\sin(\alpha)$ relation (Hönninger et al., 2004), where α denotes the elevation angle of the telescope unit. We have computed TVC NO_2 for different elevation angles and compared with TVC NO_2 as retrieved with the second approach.

The second approach is based on the Bremian advanced MAX-DOAS Retrieval Algorithm (BREAM), which was developed by Wittrock (2006) in order to retrieve tropospheric vertical columns and profiles of trace gases. The retrieval algorithm is motivated by the study of Wagner et al. (2004). Briefly, the measured slant columns of O_4 are used to retrieve aerosol information by comparing them with O_4 slant columns simulated with the radiative transfer model SCIATRAN (Rozanov et al., 2005). This information is essential to obtain accurate box air mass factors (BAMFs) for trace gases, such as NO_2. The box air mass factors are then used to retrieve the vertical profile of the trace gas from the measured slant column densities (SCDs) at different elevation angels. As the measurements provide only limited information on the vertical trace gas column, an optimal estimation method (Rodgers, 2000) is performed using an a priori profile. Further details about BREAM and the required a priori information can be found in Wittrock (2006) and Peters et al. (2012). A similar profiling technique, which is also based on the optimal estimation method, can be found in Frieß et al. (2011).

In this study, the BREAM computations of TVC NO_2 and NO_2 profiles are performed using all observations between 2° and 30° elevation angles within time intervals of 15 min each. The ocean surface spectral reflectance in the selected spectral window is assumed to be 0.05, and an appropriate a priori profile is used for the optimal estimation. Volume mixing ratios decreasing linearly with altitude are assumed for the a priori vertical NO_2 profile initially. The a priori profile is then scaled various times with scaling factors to yield a trace gas profile. The total retrieval height is 4 km with a retrieval grid size of 50 m, resulting in 80 layers. More details about the settings used for BREAM can be found in Peters et al. (2012).

As a quality criterion of TVC NO_2 and profiles as retrieved from BREAM, computations are only performed when the correlation coefficient between the measured and simulated O_4 slant columns is higher than 0.6 and when the number of elevation angles of one scanning sequence is larger than 10. The former threshold value has been selected to exclude measurements that are affected by the own ship's plume (e.g. resulting in negative SCDs). Even if the SCDs affected by an elevated exhaust plume are not negative, but obtained by using such an influenced zenith sky measurement as reference spectrum, they are not included in the retrieval of TVC NO_2 and vertical profiles from BREAM, as the correlation criterion will not be fulfilled. As we here focus on the comparison between the two described approaches, the values obtained from the geometrical approximation are shown using the same quality criteria as for BREAM.

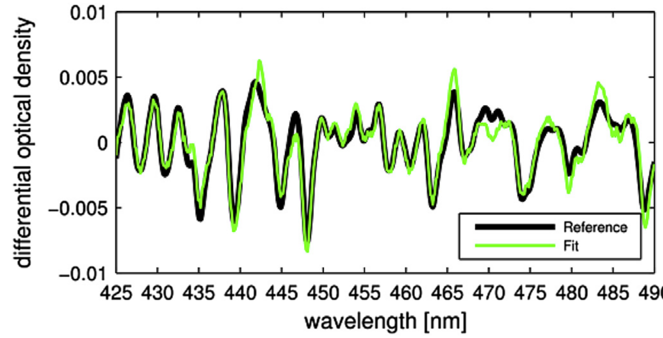

Fig. 4. Fit results of the NO_2 fit using the "adapted" settings for the morning of 17th November 2011 (23:32 UT) under elevated NO_2 pollution (SCD = 3.75×10^{16} molec cm^{-2}). The RMS of the residuals is 7.5×10^{-4}. Here, the optical density of the reference (differential absorption cross-section, scaled by the retrieved SCD, black line) and fit (reference + residual, green line) are retrieved at 2° elevation angle and at 78.13° solar zenith angle. Further explanations and definitions are given in the text. (For interpretation of the references to color in this figure legend, the reader is referred to the web version of this article.)

4. Results and discussion

4.1. Tropospheric NO_2 slant column densities

The "standard" set up for fitting as applied during the CINDI campaign (Roscoe et al., 2010) is compared with a fit including the absorption of liquid water (Pope and Fry, 1997) and the correction spectrum accounting for liquid water and effects of VRS (Peters et al., 2014), here referred to as "adapted" settings (see Fig. 3 and Table 1). In Fig. 3, the differential optical density of the NO_2 fit is plotted against the differential optical density of the NO_2 reference

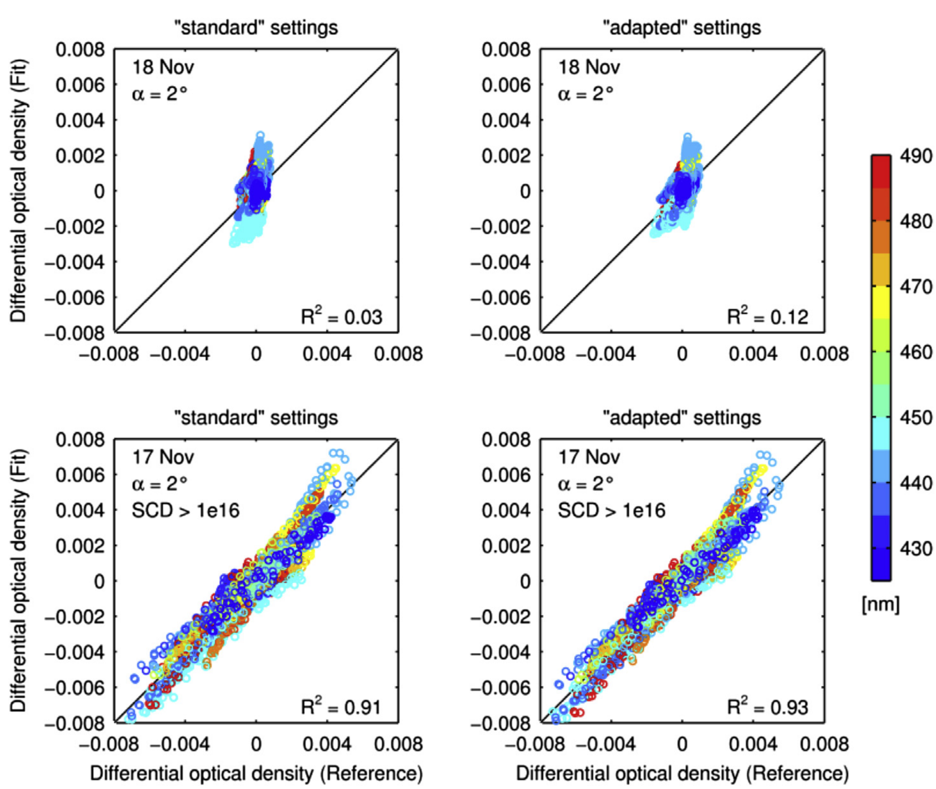

Fig. 3. Scatter plots of differential optical density (Fit) vs. differential optical density (Reference) for the NO_2 "standard" settings (left) and "adapted" settings including the absorption of liquid water and an empirical correction spectrum for liquid water and VRS (right). Here, the scatter plots are shown for the NO_2 fits including only $\alpha = 2°$ measurements for an unpolluted (top) and polluted case (bottom). Further explanations and definitions are given in the text.

for an unpolluted (top) and polluted case (bottom) as a function of wavelength. Here, the reference is defined as the scaled cross section (with the slant column as scaling factor) and the fit is defined as the scaled cross section including the fit residuals. For the unpolluted case, all measurements at $\alpha = 2°$ taken on the 18th November are included in the scatter plot. The polluted case has been selected on 17th November and includes all measurements at $\alpha = 2°$ that exceed a value for the NO_2 SCD of 1×10^{16} molec cm^{-2}. The left plots in the figure represent the results using "standard" settings, whereas the right plots show the results using the "adapted" settings. There is some degree of improvement (higher r^2 values) in the NO_2 fit quality when including the absorption of liquid water and the empirical correction spectrum for an elevation angle of 2°. This is in good agreement with the recent study by Peters et al. (2014).

While all measurements $\alpha = 2°$ from 17th November are included in Fig. 3 (bottom), only one exemplary measurement at $\alpha = 2°$ is shown in Fig. 4 for the morning of 17th November, when the RV Sonne left the dense shipping lane connecting Singapore and East China. The measurement was taken at a solar zenith angle of 78.13° and the obtained SCD is 3.75×10^{16} molec cm^{-2} with an RMS of 7.5×10^{-4}. There is good correlation between the reference (black line) and the fit (green line). Compared to the standard settings, however, there is only minor improvement, which is not directly visible in the fit result (not shown).

The results of Figs. 3 and 4 suggest that the overall fit quality for cases with elevated NO_2 levels is good enough to retrieve NO_2 SCDs and subsequently estimate TVC NO_2 via the geometric approach and BREAM.

A detection limit for NO_2 slant columns from MAX-DOAS measurements in the open ocean has recently been estimated by Peters et al. (2012). RMS values from the best NO_2 fits in the order of 1×10^{-4} were used to derive an upper detection limit of 2×10^{15} molec cm^{-2}. As we find similar RMS values for the best fits in this study, their detection limit can also be assumed here.

The color-coded time series of the obtained NO_2 SCDs are shown in Figs. 5b–7b for the individual days. Obviously, the highest values are observed at the lowest elevation angles, whereas the lowest values are found at the highest elevation angles, indicating that largest amounts of tropospheric NO_2 are located close to the

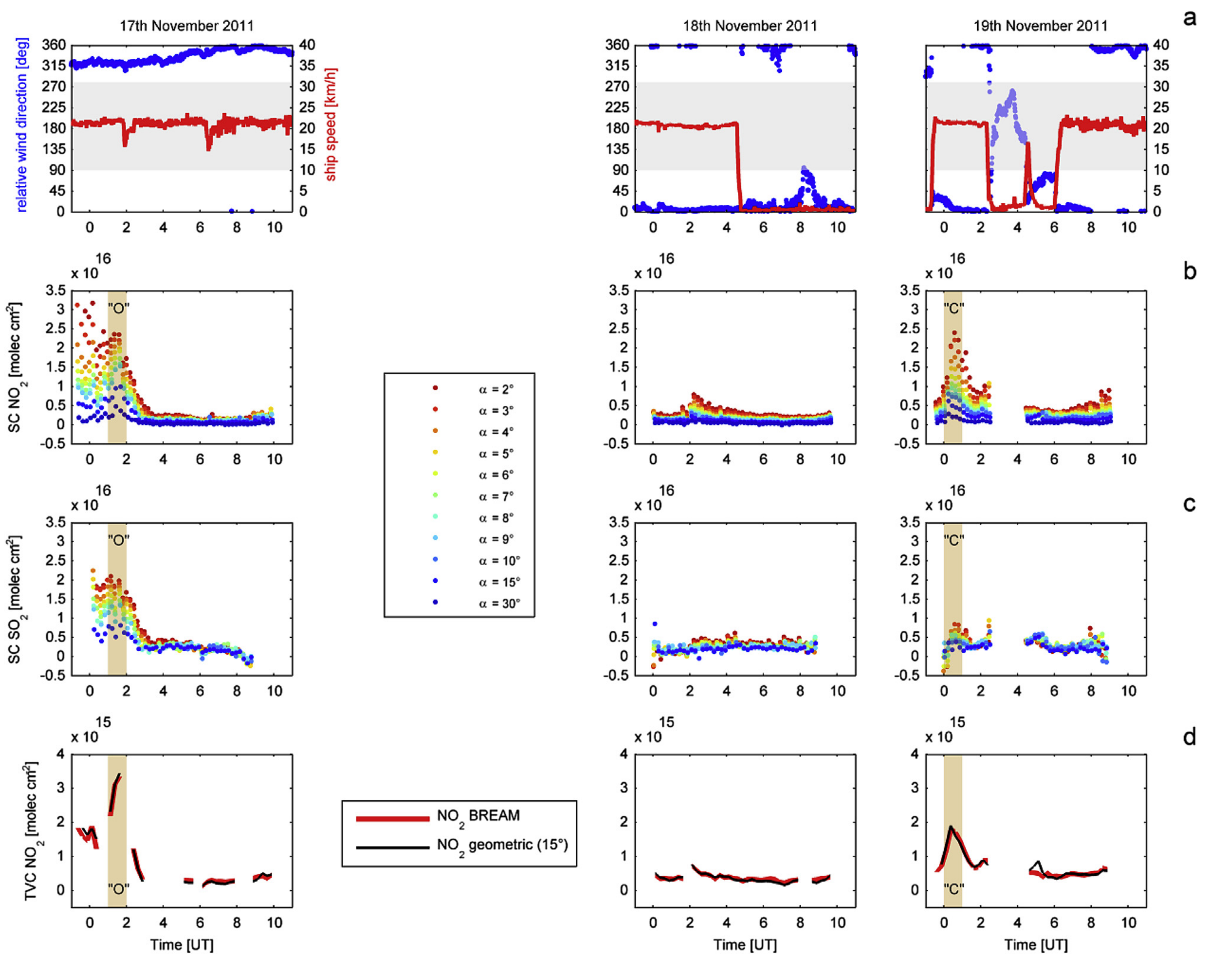

Fig. 5. Time series of ship's data and tropospheric NO_2 and SO_2 amounts for the days 17th, 18th, and 19th November 2011. Relative wind direction (blue dots) and ship speed (red line) as downloaded from the ship's database (a). The transparent gray area highlights the range of relative wind directions between 90° and 280°, which was used for data screening of the measured MAX-DOAS spectra. Tropospheric NO_2 (b) and SO_2 (c) SCDs as retrieved from the MAX-DOAS measurements at different elevation angles. NO_2 tropospheric vertical columns (TVC NO_2) as obtained from BREAM (red) and from the geometric approach using $\alpha = 15°$ (black) (d). The brown shaded areas in panels (b), (c), and (d) indicate the time of backward trajectory calculations (±30 min) as indicated in Fig. 1, where "O" and "C" denote the origin of air masses from the ocean and coast, respectively. (For interpretation of the references to color in this figure legend, the reader is referred to the web version of this article.)

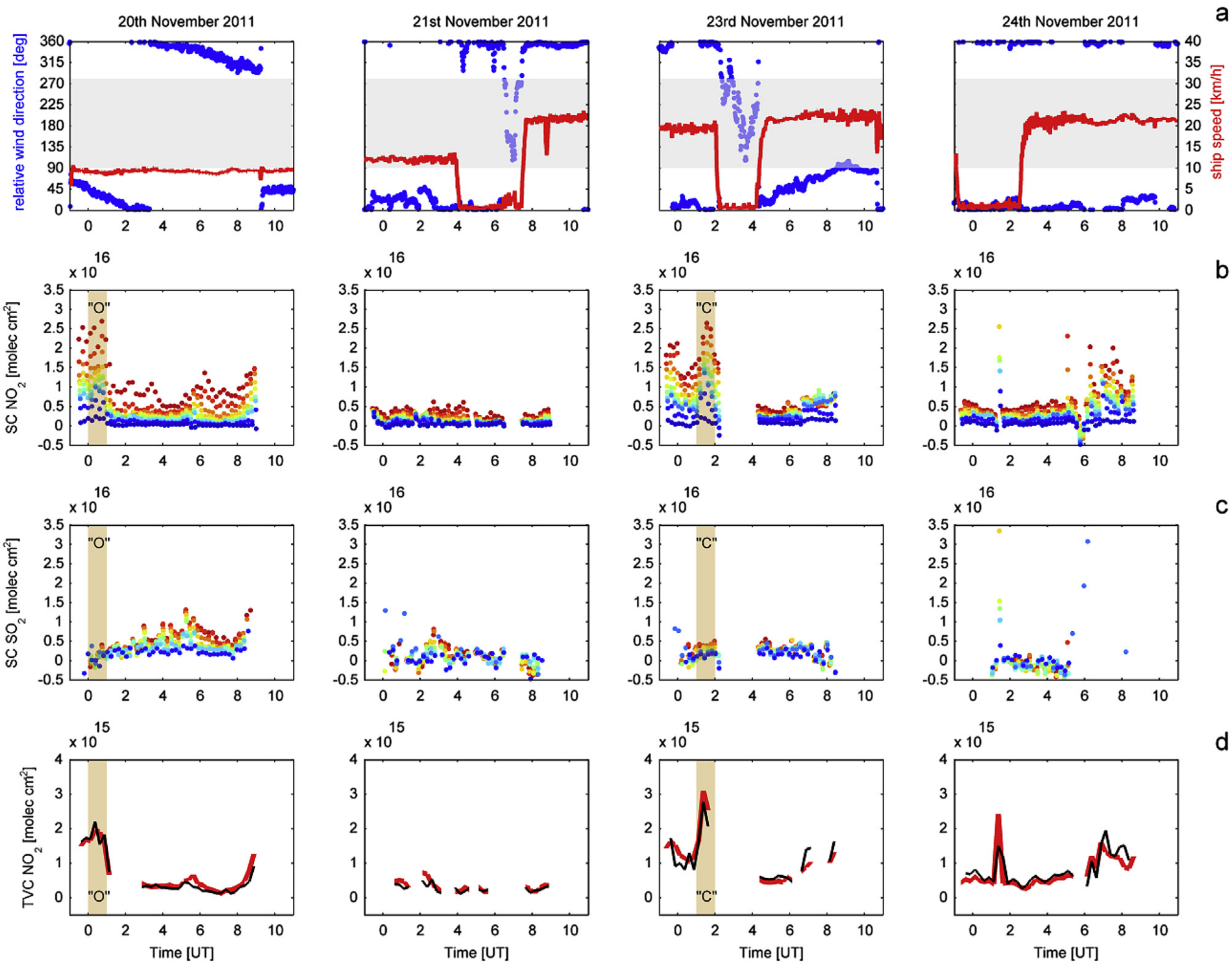

Fig. 6. Same as Fig. 5, but for the days 20th, 21st, 23rd, and 24th November 2011.

ground. The lowest NO_2 SCDs are observed when the ship was far away from the coast and in a sufficiently large distance to other ships. For instance, the low values in the afternoon of 17th November and during almost the entire day of 18th November have been observed while the ship left the dense traffic lane and headed towards the coast of Borneo (see Fig. 1). On all other days, there was at least one peak in the time series of NO_2 SCDs. For most of the time when higher values of NO_2 SCDs are found, the ship was either in proximity to the coast or close to other vessels. Interestingly, the highest values exceeding 2×10^{16} molec cm^{-2} at $\alpha = 2°$ were observed in the morning hours of 19th, 20th, and 23rd November. This is in good agreement with Takashima et al. (2012), as they have also highlighted a diurnal variation close to the coast with higher values in the morning.

Whether these elevated levels of NO_2 are released by anthropogenic emission sources or produced by microbial activity of soils is difficult to judge. However, the sharp drop throughout the day leads to the assumption that the emission strength undergoes a daily cycle. On the other hand, photolysis of NO_2 with increasing solar UV radiation could also determine the sharp drop of NO_2 amounts. The fast photolysis of NO_2, which largely controls tropospheric O_3 formation, is important for the production of hydroxyl (OH) radicals (Crutzen and Lelieveld, 2001). These secondary products of ozone photolysis could additionally influence the removal of tropospheric NO_x and thus, explain the sharp decrease in the morning.

We note that the negative SCDs which are occasionally observed, especially for larger elevation angles, could be attributed to unfavorable zenith measurements (influence of NO_2 from an elevated plume or from the ship's smoke stack), which are used for the retrieval of the differential SCDs. However, for the computation of vertical columns and profiles with BREAM, these measurements are not included.

The ship-based MAX-DOAS measurements indicate increased tropospheric amounts of NO_2 in the morning of 17th November, when the ship was leaving a busy shipping lane (see Fig. 5b). As no other sources than from international shipping can be expected in this area, these elevated NO_2 levels can be clearly attributed to shipping emissions released by other vessels moving in the dense shipping lane. Moreover, air masses originating from the north brought air passing over the ship track into the instrument's field of view. When the RV Sonne left the shipping lane and moved towards the coast of Borneo, these increased NO_2 amounts disappeared and concentrations in the boundary layer reached low values.

4.2. Tropospheric SO_2 slant column densities

In order to compare the daily cycle of NO_2 with another trace gas emitted from ship stacks, we have also retrieved SO_2 from the MAX-DOAS measurements. As NO_2 and SO_2 both have a relatively short lifetime in the tropical boundary layer of <10 h (e.g. Beirle et al., 2011) and >10 h (Lee et al., 2011), respectively, one would expect

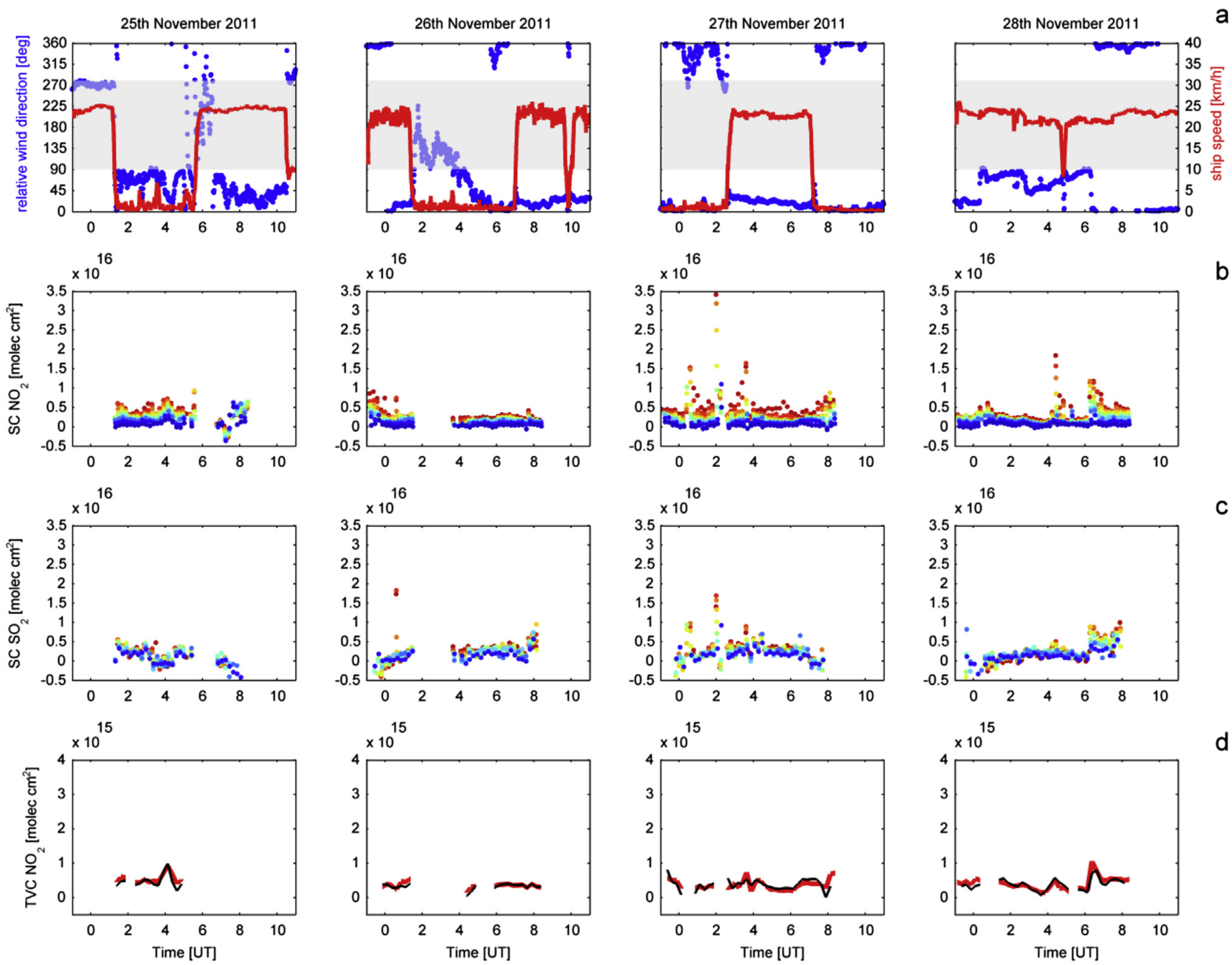

Fig. 7. Same as Fig. 5, but for the days 25th, 26th, 27th, and 28th November 2011.

high temporal correlation between the two time series of NO_2 and SO_2 for 17th November 2011.

Exemplary fit results of the SO_2 fit are shown in Fig. 8. The spectral measurement was taken on 17th November at 2° elevation angle and 53.33° solar zenith angle. In general, there is a good agreement between the reference (black line) and the fit (red line). The agreement is best for the lower wavelengths where the differential optical depth is larger. However, differences are larger for cases with lower tropospheric SO_2 amounts (not shown).

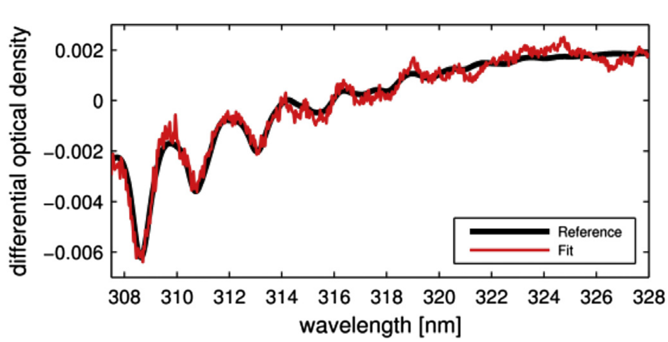

Fig. 8. Fit results of the SO_2 fit for a single measured spectrum taken in the morning of 17th November 2011 (01:20 UT) under elevated SO_2 pollution (SCD = 1.84×10^{16} molec cm^{-2}). The RMS of the residuals is 5×10^{-4}. Here, the optical density of the reference (black line) and fit (red line) are retrieved at 2° elevation angle and at 53.33° solar zenith angle. Further explanations and definitions are given in the text. (For interpretation of the references to color in this figure legend, the reader is referred to the web version of this article.)

For the case of SO_2, we found that RMS values for the best fits are 2×10^{-4} and thus, the best detection limit of 4×10^{15} molec cm^{-2} is two times as large as for NO_2, which might be related to both reduced light path length and sensitivity in the UV fitting window.

The time series of tropospheric SO_2 SCDs are shown in Figs. 5c–7c for all days when ship-based MAX-DOAS measurements were performed. In general, the values are rather low on most days as no larger sources are expected in this region. However, elevated values of SO_2 SCDs exceeding 2×10^{16} molec cm^{-2} at $\alpha = 2°$ are found in the morning of 17th November, when the ship was moving in proximity to the dense shipping lane. The values of SO_2 SCDs in the lowest elevation angles are slightly lower but in general consistent with NO_2 SCDs. This is in good agreement with the findings by Eyring et al. (2010) as they also report higher NO_2 than SO_2 from shipping emissions. DOAS measurements from an airborne platform in the Baltic Sea indicated slightly higher amounts of SO_2 than NO_2 from shipping emissions (Berg et al., 2012). However, these measurements were performed in the proximity to the individual ships and thus, reflected rather fresh smoke plumes having larger NO/NO_x ratio. Indeed, the NO_2/SO_2 ratio could also be influenced by differences in the sulfur content of the shipping fuels.

The sharp decrease of SO_2 on 17th November around 02:00 UT is also consistent with the decline in NO_2 and might be related to the separation of RV Sonne from the shipping lane (see Fig. 5b and c). In the afternoon and when the ship was moving towards the coast of Borneo, the SO_2 SCDs reached very low levels, which was also found for NO_2.

Shipping emissions from a single large vessel on 24th November are also visible from the SO_2 data. As shown in Fig. 6b for NO_2, there is an increased short-term signal of SO_2 at the same time and of similar magnitude. Such short-term signals are also found on 27th November, which might be released from other vessel moving in proximity to the RV Sonne. However, we could not identify larger ships from the video camera's records on that day and thus, these elevated values could also originate from the own ship's plume in spite of the wind direction filtering applied to the data. Another explanation for these elevated values could be the transport of SO_2 from ships that were out of sight.

On 20th November, elevated SO_2 values in the afternoon could originate from flaring at offshore oil production sites that are found in this region (e.g. Nara et al., 2014). As discussed above, NO_2 observations have also indicated elevated values on that day. However, the increased NO_2 levels, which unlike SO_2 are also found in the morning, are higher in magnitude than SO_2 amounts. On 19th and 23rd November, elevated NO_2 amounts in the morning could have originated from the nearby cities of Kuching and Kota Kinabalu, respectively. This speculation is supported by slightly elevated SO_2 values. For example, high NO_2 together with low SO_2 could arise from traffic rather than from soil microbial activity.

In Fig. 9, a color-coded scatter plot of SO_2 SCDs vs. NO_2 SCDs for the different elevation angles is shown for all measurements taken on 17th November, when the RV Sonne left the busy shipping lane in the South China Sea. For a better comparison, we have used the 30° measurements as FRS also for NO_2. The solid black line is the 1:1 line and the dashed gray lines indicate the ±20% bounds. As already discussed above, the higher values at lower elevation angles are linked to shipping emissions. Berg et al. (2012) found that SO_2 amounts are higher than NO_2 amounts in fresh plumes released from vessels in the Baltic Sea. The fact that increased NO_2 and SO_2 amounts observed in our study are in good agreement could be related to transport of polluted air masses from the North and the consequent increasing formation of NO_2 within the plume. However, we also observed cases where SO_2 SCDs were higher than NO_2 SCDs, which could be linked to rather fresh shipping emissions from vessels moving in proximity to RV Sonne. The scatter between NO_2 and SO_2 is larger for smaller trace gas amounts, which is linked to the fact that concentrations are below the estimated detection limits of 2 and 4×10^{15} molec cm^{-2}, respectively.

4.3. Tropospheric NO_2 vertical columns

In order to make the two approaches (geometric approach vs. BREAM, see Sect. 3.1.5) comparable, the TVC NO_2 values obtained from the geometric approach have been interpolated to the selected BREAM time interval (15 min).

The tropospheric NO_2 vertical columns as obtained from the geometrical approximation using the 15° (blue), 10° (green), 5° (red), and 2° (cyan) measurements are compared with TVC NO_2 as computed with BREAM for all days (Fig. 10, bottom). There is a clear indication that both 15° and 10° measurements can be applied for the geometric approach when TVC NO_2 exceeds 1.5×10^{15} molec cm^{-2}. For cases when the NO_2 amounts are rather low ($<1 \times 10^{15}$ molec cm^{-2}), the agreement between the geometric approach and BREAM is less strong and differences can be larger than ±20%. The decreasing match towards cases with lower NO_2

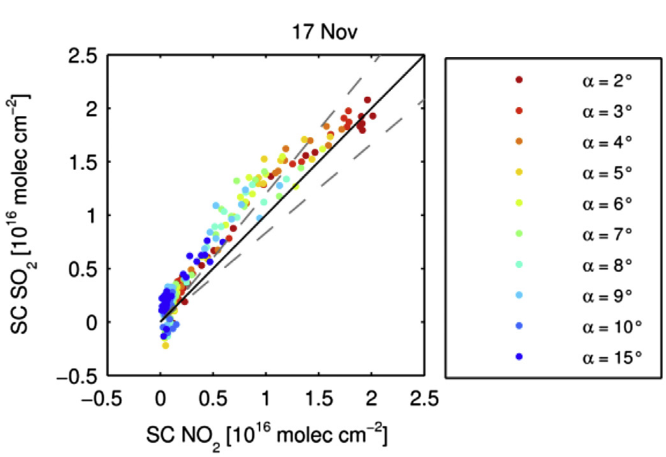

Fig. 9. Color-coded scatter plot of tropospheric SO_2 SCDs vs. NO_2 SCDs on 17th November. (For interpretation of the references to color in this figure legend, the reader is referred to the web version of this article.)

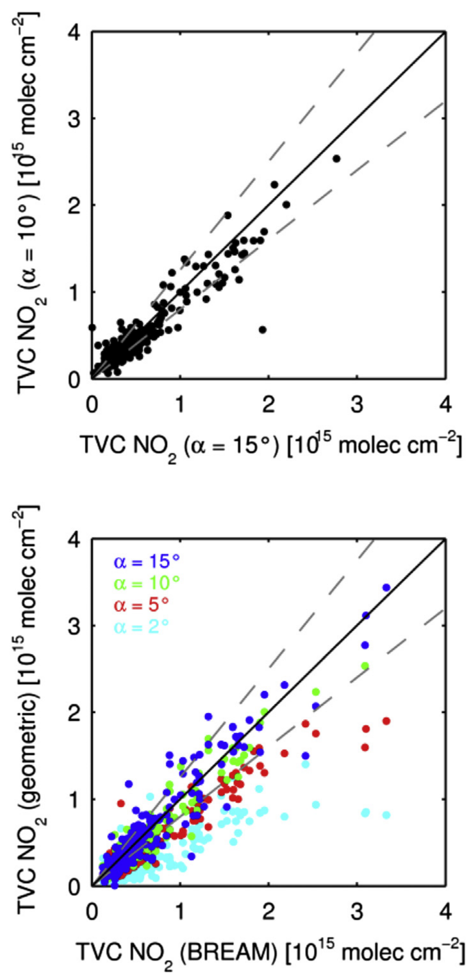

Fig. 10. Scatter plots of TVC NO_2 as obtained from the geometric approach using $\alpha = 10°$ against $\alpha = 15°$ (upper) and TVC NO_2 retrieved by the geometric approach against TVC NO_2 computed by BREAM, where $\alpha = 2°$, $\alpha = 5°$, $\alpha = 10°$, and $\alpha = 15°$ are shown in cyan, red, green, and blue, respectively (lower). The solid black line is the 1:1 line and the dashed gray lines denote the ±20% difference. (For interpretation of the references to color in this figure legend, the reader is referred to the web version of this article.)

concentrations might be an artifact of the lower fit quality (see Fig. 3), which impacts less on BREAM which is using information from all viewing angles. We found that TVC NO_2 is underestimated when the 5° (red) and 2° (cyan) measurements are used for the geometric approach. This can be explained by the fact that the tropospheric light path is shorter than assumed in the geometric approximation when the last scattering point is located within the NO_2 layer.

In the upper panel of Fig. 10, the comparison between the geometric approach using the 15° and 10° measurements is shown. Clearly, TVC NO_2 as computed from both elevation angles are in good agreement, suggesting that in these viewing directions, the last scattering point is generally above the NO_2 layer. Recent land-based MAX-DOAS campaigns have shown that 30° elevation angles are the most appropriate measurements for the geometric approach (Brinksma et al., 2008; Halla et al., 2011). However, due to the lower boundary layer height over the sea and thus, less vertical extent of NO_2, both 15° and 10° measurements seem to work well for the conversion of SCDs into TVC NO_2 in our data. Results from the radiosonde measurements performed during the SHIVA ship cruise indicate that the marine boundary layer height was lower than 500 m during daytime (Fuhlbrügge et al., 2014). There is a clear preference in using these measurements as the sensitivity for tropospheric NO_2 is much larger compared to 30° as a result of the longer light path through the boundary layer.

The time series of TVC NO_2 as obtained from the geometric approach using the 15° (red) measurements and from BREAM calculations are shown in Figs. 5d–7d. There is overall good agreement between the two time series found for most of the days. For the TVC NO_2 values from BREAM, there are some data gaps, which result from the selected time interval (15 min), threshold value for the correlation between measured and simulated O_4 slant columns ($r > 0.6$), and a minimum value for the number of elevation angles (10) within one time interval. We note that these data gaps indicate unfavorable conditions (e.g. clouds or pollution from the smoke stack in the field of view) and the TVC NO_2 obtained from the geometric approach yield unexpected high and negative values for some of these cases.

On 17th, 19th, 20th, and 23rd November, TVC NO_2 amounts of up to 3.5×10^{15} molec cm^{-2} were observed in the morning hours by both approaches (geometric vs. BREAM). During the previous TransBrom campaign (Peters et al., 2012), the highest values of TVC NO_2 (up to 2×10^{15} molec cm^{-2}) were also observed close to the coast and are in good agreement with the values observed during SHIVA. In order to investigate the origin of these elevated levels, backward trajectories were calculated for the time of peak values. The backward trajectories for these cases are shown in Fig. 1 and indicate the origin of air masses.

For instance, air masses coming from the north crossed the track of RV Sonne in the morning of 17th November. These air masses moved through the dense shipping lane connecting Singapore and coastal cities of eastern China, which bring elevated NO_2 levels from shipping emissions to the proximity of RV Sonne.

Significant NO_2 signals from international shipping have recently been identified by the evaluation of SCIAMACHY and GOME-2 satellite measurements (Beirle et al., 2004; Richter et al., 2004, 2011). Among other shipping lanes, the dense one in the South China Sea can be clearly seen from the long-term mean tropospheric NO_2 fields. De Ruyter De Wild et al. (2012) retrieved NO_2 column densities from the GOME, SCIAMACHY, OMI, and GOME-2 instruments to analyze trends over international shipping lanes. They found increasing trends of NO_2 between 2003 and 2008 over the major shipping lanes with annual running means of TVC NO_2 reaching up to 0.7×10^{15} molec cm^{-2} in the South China Sea. The trend reversed in 2008 as a consequence of the economic crisis and the linked decreased trade volume. In comparison to our MAX-DOAS results, the lower values obtained from satellite instruments are probably related to the averaging over large pixels.

Backward trajectories on the 19th and 23rd November reveal that air masses originated from the coast of Borneo. In the case of 19th November, the emissions of NO_x could be related to anthropogenic emissions from Kuching, which is the largest city on Borneo Island. The same is true for 23rd November, when air masses again originated from the coast and the city Kota Kinabalu.

The diurnal variation in TVC NO_2 shows a decrease during daytime. In addition to the enhanced photolysis of NO_2 with increasing solar UV radiation and faster removal of NO_x due to the reaction with OH, this could also be a consequence of the increased stomata uptake of NO_2 by plants throughout the day. Ganguly et al. (2009) suggested an increased NO_x uptake with increasing solar radiation in a tropical mangrove forest. During the night, the leaf stomata close and reduce NO_x uptake. Hence, the enhanced levels in observed TVC NO_2 in the morning hours could emerge due to the inactive nighttime stomata. The removal of NO_2 within the first few hours after sunrise could thus at least in part be attributed to the stomatal activity of plants during day.

The diurnal cycle in TVC NO_2 can also be seen from satellite observations. Five-year averages (2007–2011) of TVC NO_2 retrieved from the GOME-2 (9:30 LT) and OMI (13:30 LT) instruments for November 2011 are shown in Fig. 11. The difference GOME-2 minus OMI TVC NO_2 underlines the fact that higher values are observed in the morning hours close to the coast, whereas no significant pattern is observed for the remote regions of the South China and Sulu Sea. In regions where the MAX-DOAS instrument on board RV Sonne observed the distinct daily NO_2 cycle, the differences between the two satellite data are larger than 0.5×10^{15} molec cm^{-2}.

Differences in satellite-derived tropospheric NO_2 over shipping lanes between morning and afternoon have previously been discussed in Franke et al. (2009). They also found higher NO_2 amounts in the morning observed from SCIAMACHY and relate these to the diurnal cycle of NO_2, which is consistent with model simulations.

We note that the differences observed in the proximity of the coast are representative for this time of the season, where no significant sources of NO_x other than anthropogenic and soil are found close to the ground. However, higher values of TVC NO_2 in the afternoon are expected during the biomass burning season.

In addition to the elevated TVC NO_2 originating from the coast, the MAX-DOAS measurements include some observations of sharp peaks in the open sea. The most striking temporary increase in TVC NO_2 far away from any coast was observed in the morning of 24th November (see Fig. 6d). The video camera recordings revealed that this was a large vessel in the proximity to RV Sonne (not shown).

In Fig. 12, color-coded TVC NO_2 values as computed with BREAM are plotted along the ship track. Clearly, the lowest (highest) values are found in the open (coastal) waters of the South China and Sulu Sea. Increased NO_2 amounts in the open sea are the result of shipping emissions from other vessels observed by the MAX-DOAS instrument.

4.4. Tropospheric NO_2 profiles

The tropospheric NO_2 columns do not provide information about the vertical distribution of NO_2 and thus, a further step towards achieving this information is the retrieval of NO_2 profiles with BREAM (see Sect. 3.1.5). As the boundary layer height is well below 4 km in the tropics (e.g. Luo et al., 2014), the profile retrieval is expected to reflect all tropospheric NO_2 produced from soil microbial activity and anthropogenic combustion processes. However, NO_x from lightning might not be included in the obtained vertical profiles, as we expect NO_x from lightning to be emitted into higher

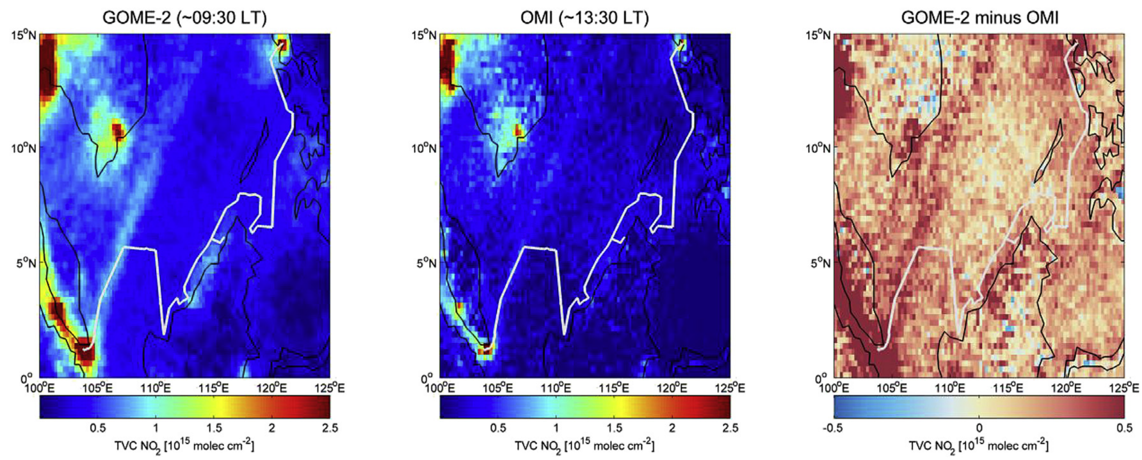

Fig. 11. Monthly gridded (0.5° × 0.5°) means of TVC NO_2 as retrieved from GOME-2 (left) and OMI (middle) for November (2007–2011). The right panel displays the differences between TVC NO_2 from GOME-2 minus TVC NO_2 from OMI.

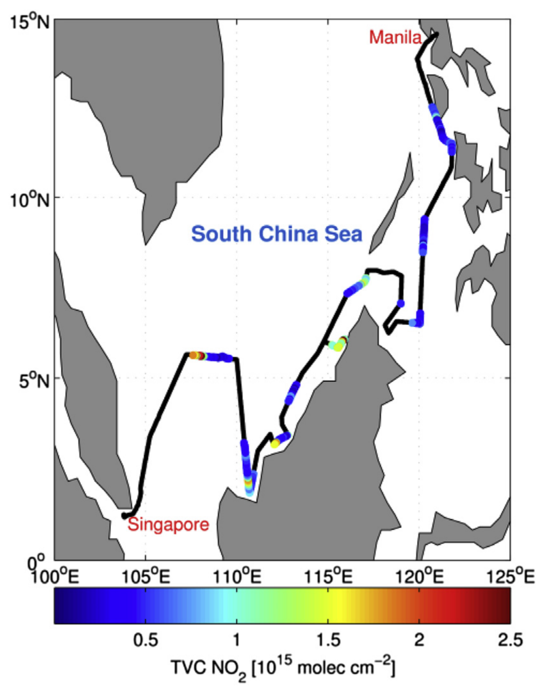

Fig. 12. Geographical map of color-coded TVC NO_2 as obtained from BREAM. (For interpretation of the references to color in this figure legend, the reader is referred to the web version of this article.)

altitudes where the sensitivity of the MAX-DOAS observations is small.

The retrieved profiles are shown in Fig. 13 for two exemplary days (17th and 23rd November). The gaps between the single profiles are the result of the limitations as already outlined in Sect. 4.2. Wittrock (2006) has shown that the errors of the volume mixing ratios in the lowermost 500 m are within 25%. The highest observed NO_2 mixing ratios exceeding 1 ppbv are found close to the surface when the RV Sonne was moving in a dense shipping lane (17th November) or along the coast (23rd November). These elevated NO_2 mixing ratios are in good agreement with the highest values (~0.8 ppbv) reported by Peters et al. (2012).

The lowest NO_2 mixing ratios close to the ground are <30–50 pptv and can be as high as 100 pptv, as observed on 18th November, for instance (not shown). This is in good agreement with the former ship-based studies by Peters et al. (2012) and Takashima et al. (2012), suggesting boundary layer background mixing ratios of <50 and up to 200 pptv, respectively. The explanation of the lower background values found in our study could be related to the improvements achieved using the adapted fit, which increases the signal-to-noise ratio.

5. Summary and conclusions

Ship-based Multi-Axis Differential Optical Absorption Spectroscopy (MAX-DOAS) measurements performed in the South China and Sulu Sea in November 2011 have been used to retrieve tropospheric NO_2 vertical columns (TVC NO_2) and slant column densities (SCDs) of SO_2.

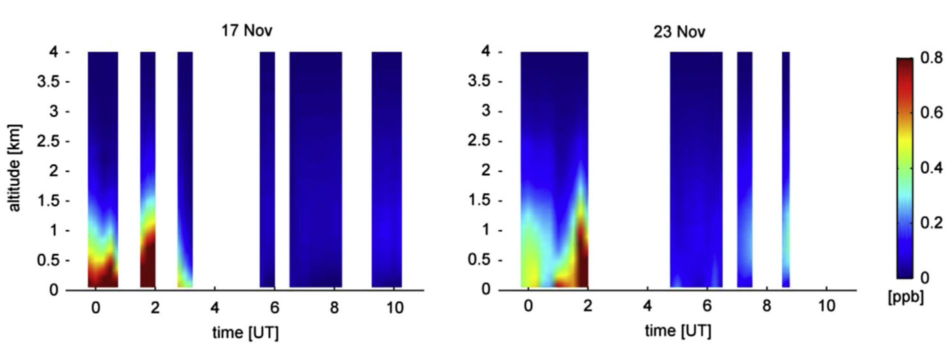

Fig. 13. Exemplary vertical profiles of NO_2 mixing ratios for 17th and 23rd November as obtained from BREAM.

For NO_2, we have used the cross-sections and the 425–490 nm fitting window as suggested in Roscoe et al. (2010) but adapted the NO_2 fit by including a cross-section for liquid water and an empirical correction spectrum as discussed in Peters et al. (2014). As a result, the fit quality slightly improved, especially for the lowest elevation angles and when NO_2 amounts are rather low.

The time series of tropospheric NO_2 slant column densities (SCDs), which have been obtained by using a zenith measurement close in time as Fraunhofer reference spectrum (FRS), indicate that the highest levels of NO_2 are found at the lowest elevation angles. The conversion of SCDs into the more commonly used TVC NO_2 is based on two different approaches.

The simple geometric approach was tested for different elevation angles and compared with TVC NO_2 as computed from the vertical profiles inverted with BREAM. The comparison between TVC NO_2 as obtained from 10° to 15° measurements for SZA <75° showed that both can be used to retrieve TVC NO_2 from MAX-DOAS measurements in the tropical marine environment with values comparable to what is derived by a full inversion. Geometric values from even lower elevations underestimate the true columns as the last scattering point moves into the layer of enhanced NO_2.

Although the NO_2 amounts in the marine environment of Southeast Asia are rather low when compared to larger cities or intensive biomass burning regions, the MAX-DOAS measurements on board the RV Sonne yielded some interesting insights in the spatio-temporal patterns of tropospheric NO_2. We expected very low values, but occasionally identified increased NO_2 amounts, mostly resulting from fuel combustion and possibly also from soil microbial activity – but to a lesser proportion than from anthropogenic activities. These peaks, which predominantly occurred in the morning hours, disappeared quite soon after – most probably due to fast photolysis of NO_2 with increasing solar UV radiation.

The results show that the boundary layer values of NO_2 are well below 100 pptv and <30 pptv in the open waters of the South China and Sulu Sea. However, mixing ratios exceeded 0.8 ppbv when the RV Sonne was heading along the coast or in proximity to other vessels.

In addition to NO_2, we have also retrieved SO_2 SCDs in a fitting window between 307.5 and 328 nm. We report increased tropospheric SO_2 SCDs in the lowest layers when the RV Sonne was in proximity to a dense shipping lane and thus, attribute these values to both fresh and aged plumes released from larger vessels. The values are in general agreement with NO_2 SCDs, indicating comparable magnitudes of shipping NO_x and SO_2.

From our measurements it is clear, that ship traffic has a large impact on pollutant levels in the South China Sea, at least in the vicinity of the busy shipping lanes.

Acknowledgments

The ship's data were generated or collected within the framework of the German Research Project SHIVA-SONNE, funded by the BMBF and the EU Project SHIVA. Financial assistance was also provided by the EU SHIVA Project (226224-FP7-ENV-2008-1) and from the Project SOPRAN (03F0662F), funded by BMBF. S. F. Schreier acknowledges funding by the Earth System Science Research School (ESSReS). We acknowledge the use of GOME-2 lv1 data from EUMETSAT and OMI lv1 data from NASA. The HYSPLIT online tool from NOAA was used for the calculation of backward trajectories. Lastly, the authors wish to thank two anonymous reviewers for their useful comments.

Appendix A. Supplementary data

Supplementary data related to this article can be found at http://dx.doi.org/10.1016/j.atmosenv.2014.12.015.

References

Achard, F., Eva, H.D., Stibig, H.J., Mayaux, P., Gallego, J., Richards, T., Malingreau, J.P., 2002. Determination of deforestation rates of the world's humid tropical forests. Science 297, 999–1002.

Beirle, S., Platt, U., von Glasow, R., Wenig, M., Wagner, T., 2004. Estimate of nitrogen oxide emissions from shipping by satellite remote sensing. Geophys. Res. Lett. 31, L18102. http://dx.doi.org/10.1029/2004GL020312.

Beirle, S., Boersma, K.F., Platt, U., Lawrence, M.G., Wagner, T., 2011. Megacity emissions and lifetimes of nitrogen oxides probed from space. Science 333, 1737–1739.

Berg, N., Mellqvist, J., Jalkanen, J.-P., Balzani, J., 2012. Ship emissions of SO_2 and NO_2: DOAS measurements from airborne platforms. Atmos. Meas. Tech. 5, 1085–1098. http://dx.doi.org/10.5194/amt-5-1085-2012.

Berglen, T.F., Bernsten, T.K., Isaksen, I.S.A., Sundet, J.K., 2004. A global model of the coupled sulfur/oxidant chemistry in the troposphere: the sulfur cycle. J. Geophys. Res. 109, D19310. http://dx.doi.org/10.1029/2003JD003948.

Bogumil, K., Orphal, J., Homann, T., Voigt, S., Spietz, P., Fleischmann, O.C., Vogel, A., Hartmann, M., Kromminga, H., Bovensmann, H., Frerick, J., Burrows, J.P., 2003. Measurements of molecular absorption spectra with the SCIAMACHY preflight model: instrument characterization and reference data for atmospheric remote-sensing in the 230–2380 nm region. J. Photochem. Photobiol. A 157, 167–184.

Brewer, A.C., McElroy, C.T., Kerr, J.B., 1973. Nitrogen dioxide concentrations in the atmosphere. Nature 246, 129–133.

Brinksma, E.J., Pinardi, G., Braak, R., Volten, H., Richter, A., Schoenhardt, A., Van Roozendael, M., Fayt, C., Hermans, C., Dirksen, R.J., Vlemmix, T., Berkhout, A.J.C., Swart, D.P.J., Oetjen, H., Wittrock, F., Wagner, T., Ibrahim, O.W., de Leeuw, G., Moerman, M., Curier, R.L., Celarier, E.A., Knap, W.H., Veefkind, J.P., Eskes, H.J., Allaart, M., Rothe, R., Piters, A.J.M., Levelt, P.F., 2008. The 2005 and 2006 DANDELIONS NO_2 and aerosol intercomparison campaigns. J. Geophys. Res. 113, D16S46. http://dx.doi.org/10.1029/2007JD008808.

Browell, E.V., Fenn, M.A., Butler, C.F., Grant, W.B., Ismail, S., Ferrare, R.A., Kooi, S.A., Brackett, V.G., Clayton, M.B., Avery, M.A., Barrick, J.D.W., Fuelberg, H.E., Maloney, J.C., Newell, R.E., Zhu, Y., Mahoney, M.J., Anderson, B.E., Blake, D.R., Brune, W.H., Heikes, B.G., Sachse, G.W., Singh, H.B., Talbot, R.W., 2001. Large-scale air mass characteristics observed over the remote tropical Pacific Ocean during March–April 1999: results from PEM Tropics B Field Experiment. J. Geophys. Res. 106, 32481–32501.

Crutzen, P.J., Lelieveld, J., 2001. Human impacts on atmospheric chemistry. Annu. Rev. Earth Planet. Sci. 29, 17–45.

De Ruyter De Wildt, M., Eskes, H., Boersma, K.F., 2012. The global economic cycle and satellite-derived NO_2 trends over shipping lanes. Geophys. Res. Lett. 39.

Deutschmann, T., Beirle, S., Frieß, U., Grzegorski, M., Kern, C., Kritten, L., Platt, U., Prados-Román, C., Puklite, J., Wagner, T., Werner, B., Pfeilsticker, K., 2011. The Monte Carlo atmospheric radiative transfer model McArtim: Introduction and validation of Jacobians and 3D features. J. Quant. Spectrosc. Radiat. Trans. 112, 1119–1137. http://dx.doi.org/10.1016/j.jqsrt.2010.12.009.

Endresen, Ø., Bakke, J., Sørgård, E., Berglen, T.F., Holmvang, P., 2005. Improved modelling of ship SO_2 emissions – a fuel based approach. Atmos. Environ. 39, 3621–3628.

Eyring, V., Isaksen, I.S.A., Berntsen, T., Collins, W.J., Corbett, J.J., Endresen, Ø., Grainger, R.G., Moldanova, J., Schlager, H., Stevenson, D.S., 2010. Transport impacts on atmosphere and climate: shipping. Atmos. Environ. 44, 4735–4771. http://dx.doi.org/10.1016/j.atmosenv.2009.04.059.

Franke, K., Richter, A., Bovensmann, H., Eyring, V., Jockel, P., Hoor, P., Burrows, J.P., 2009. Ship emitted NO_2 in the Indian Ocean: comparison of model results with satellite data. Atmos. Chem. Phys. 9, 7289–7301. http://dx.doi.org/10.5194/acp-9-7289-2009.

Frieß, U., Sihler, H., Sander, R., Pöhler, D., Yilmaz, S., Platt, U., 2011. The vertical distribution of BrO and aerosols in the Arctic: measurements by active and passive differential optical absorption spectroscopy. J. Geophys. Res. 116, D00R04. http://dx.doi.org/10.1029/2011JD015938.

Fuhlbrügge, S., Quack, B., Krüger, K., Tegtmeier, S., Atlas, E., Raimund, R., Hepach, H., Shi, Q., 2014. The contribution of oceanic halocarbons to marine and free tropospheric air over the South China and Sulu Seas (in preparation).

Ganguly, D., Dey, M., Sen, S., Jana, T.K., 2009. Biosphere-atmosphere exchange of NO_x in the tropical mangrove forest. J. Geophys. Res. 114, G04014. http://dx.doi.org/10.1029/2008JG000852.

Gorshelev, V., Serdyuchenko, A., Weber, M., Chehade, W., Burrows, J.P., 2014. High spectral resolution ozone absorption cross-sections – part 1: measurements, data analysis and comparison with previous measurements around 293 K. Atmos. Meas. Tech. 7, 609–624. http://dx.doi.org/10.5194/amt-7-609-2014.

Greenblatt, G.D., Orlando, J.J., Burkholder, J.B., Ravishankara, A.R., 1990. Absorption-measurements of oxygen between 330 nm and 1140 nm. J. Geophys. Res. Atmos. 95, 18577–18582.

Großmann, K., Frieß, U., Peters, E., Wittrock, F., Lampel, J., Yilmaz, S., Tschritter, J., Sommariva, R., von Glasow, R., Quack, B., Krüger, K., Pfeilsticker, K., Platt, U., 2013. Iodine monoxide in the Western Pacific marine boundary layer. Atmos. Chem. Phys. 13, 3363–3378. http://dx.doi.org/10.5194/acp-13-3363-2013.

Halla, J.D., Wagner, T., Beirle, S., Brook, J.R., Hayden, K.L., O'Brien, J.M., Ng, A., Majonis, D., Wenig, M.O., McLaren, R., 2011. Determination of tropospheric vertical columns of NO_2 and aerosol optical properties in a rural setting using MAX-DOAS. Atmos. Chem. Phys. 11, 12475–12498. http://dx.doi.org/10.5194/

acp-11-12475-2011.
Hewitt, C.N., MacKenzie, A.R., Di Carlo, P., Di Marco, C.F., Dorsey, J.R., Evans, M., Fowler, D., Gallagher, M.W., Hopkins, J.R., Jones, C.E., Langford, B., Lee, J.D., Lewis, A.C., Lim, S.F., McQuaid, J., Misztal, P., Moller, S.J., Monks, P.S., Nemitz, E., Oram, D.E., Owen, S.M., Phillips, G.J., Pugh, T.A.M., Pyle, J.A., Reeves, C.E., Ryder, J., Siong, J., Skiba, U., Stewart, D.J., 2009. Nitrogen management is essential to prevent tropical oil palm plantations from causing ground-level ozone pollution. Proc. Natl. Acad. Sci. U. S. A. 106, 18447–18451.
Hönninger, G., von Friedeburg, C., Platt, U., 2004. Multi axis differential optical absorption spectroscopy (MAX-DOAS). Atmos. Chem. Phys. 4, 231–254.
Irie, H., Takashima, H., Kanaya, Y., Boersma, K.F., Gast, L., Wittrock, F., Brunner, D., Zhou, Y., Van Roozendael, M., 2011. Eight-component retrievals from ground-based MAX-DOAS observations. Atmos. Meas. Tech. 4, 1027–1044. http://dx.doi.org/10.5194/amt-4-1027-2011.
Lee, D.S., Köhler, I., Grobler, E., Rohrer, F., Sausen, R., Gallardo-Klenner, L., Olivier, J.G.J., Dentener, F.J., Bouwman, A.F., 1997. Estimations of global NO(x) emissions and their uncertainties. Atmos. Environ. 31, 1735–1749.
Lee, C., Martin, R.V., van Donkelaar, A., Lee, H., Dickerson, R.R., Hains, J.C., Krotkov, N., Richter, A., Vinnikov, K., Schwab, J.J., 2011. SO_2 emissions and lifetimes: estimates from inverse modeling using in situ and global, space-based (SCIAMACHY and OMI) observations. J. Geophys. Res. 116, D06304. http://dx.doi.org/10.1029/2010JD014758.
Luo, T., Yuan, R., Wang, Z., 2014. Lidar-based remote sensing of atmospheric boundary layer height over land and ocean. Atmos. Meas. Tech. 7, 173–182. http://dx.doi.org/10.5194/amt-7-173-2014.
MacKenzie, A.R., Langford, B., Pugh, T.A.M., Robinson, N., Misztal, P.K., Heard, D.E., Lee, J.D., Lewis, A.C., Jones, C.E., Hopkins, J.R., Phillips, G., Monks, P.S., Karunaharan, A., Hornsby, K.E., Nicolas-Perea, V., Coe, H., Gabey, A.M., Gallagher, M.W., Whalley, L.K., Edwards, P.M., Evans, M.J., Stone, D., Ingham, T., Commane, R., Furneaux, K.L., McQuaid, J.B., Nemitz, E., Seng, Y., Fowler, D., Pyle, J.A., Hewitt, C.N., 2011. The atmospheric chemistry of trace gases and particulate matter emitted by different land uses in Borneo. Philos. Trans. R. Soc. B Biol. Sci. 366, 3177–3195.
Miettinen, J., Shi, C., Liew, S.C., 2011. Deforestation rates in insular Southeast Asia between 2000 and 2010. Glob. Change Biol. 17, 2261–2270.
Nara, H., Tanimoto, H., Tohjima, Y., Mukai, H., Nojiri, Y., Machida, T., 2014. Emissions of methane from offshore oil and gas platforms in Southeast Asia, Scientific Reports 4, Article number: 6503. http://dx.doi.org/10.1038/srep06503.
Noxon, J.F., 1975. Nitrogen dioxide in the stratosphere and troposphere measured by ground based absorption spectroscopy. Science 189, 547–549.
Perner, D., Platt, U., 1979. Detection of nitrous acid in the atmosphere by differential optical absorption. Geophys. Res. Lett. 6, 917–920.
Peters, E., 2013. Improved MAX-DOAS Measurements and Retrievals Focused on the Marine Boundary Layer. Ph.D.. University of Bremen, Bremen, Germany, available at http://www.doas-bremen.de/paper/diss_peters_2013.pdf (last accessed May 2014).
Peters, E., Wittrock, F., Großmann, K., Frieß, U., Richter, A., Burrows, J.P., 2012. Formaldehyde and nitrogen dioxide over the remote western Pacific Ocean: SCIAMACHY and GOME-2 validation using ship-based MAX-DOAS observations. Atmos. Chem. Phys. 12, 11179–11197.
Peters, E., Wittrock, F., Richter, A., Alvarado, L.M.A., Rozanov, V.V., Burrows, J.P., 2014. Liquid water absorption and scattering effects in DOAS retrievals over oceans. Atmos. Meas. Tech. 7, 4203–4221. http://dx.doi.org/10.5194/amt-7-4203-2014.
Pfeilsticker, K., The SHIVA Consortium, 2013. Overview on the Project SHIVA (Stratospheric Ozone: Halogen Impacts in a Varying Atmosphere): Achievements and Key Results (in preparation).
Piters, A.J.M., Boersma, K.F., Kroon, M., Hains, J.C., Van Roozendael, M., Wittrock, F., Abuhassan, N., Adams, C., Akrami, M., Allaart, M.A.F., Apituley, A., Beirle, S., Bergwerff, J.B., Berkhout, A.J.C., Brunner, D., Cede, A., Chong, J., Clémer, K., Fayt, C., Frieß, U., Gast, L.F.L., Gil-Ojeda, M., Goutail, F., Graves, R., Griesfeller, A., Großmann, K., Hemerijckx, G., Hendrick, F., Henzing, B., Herman, J., Hermans, C., Hoexum, M., van der Hoff, G.R., Irie, H., Johnston, P.V., Kanaya, Y., Kim, Y.J., Klein Baltink, H., Kreher, K., de Leeuw, G., Leigh, R., Merlaud, A., Moerman, M.M., Monks, P.S., Mount, G.H., Navarro-Comas, M., Oetjen, H., Pazmino, A., Perez-Camacho, M., Peters, E., du Piesanie, A., Pinardi, G., Puentedura, O., Richter, A., Roscoe, H.K., Schönhardt, A., Schwarzenbach, B., Shaiganfar, R., Sluis, W., Spinei, E., Stolk, A.P., Strong, K., Swart, D.P.J., Takashima, H., Vlemmix, T., Vrekoussis, M., Wagner, T., Whyte, C., Wilson, K.M., Yela, M., Yilmaz, S., Zieger, P., Zhou, Y., 2012. The Cabauw Intercomparison campaign for Nitrogen Dioxide measuring Instruments (CINDI): design, execution, and early results. Atmos. Meas. Tech. 5, 457–485. http://dx.doi.org/10.5194/amt-5-457-2012.
Platt, U., Stutz, J., 2008. Differential Optical Absorption Spectroscopy, Physics of Earth and Space Environments. Springer, Berlin, Germany.
Pope, R.M., Fry, E.S., 1997. Absorption spectrum (380–700 nm) of pure water. II. Integrating cavity measurements. Appl. Opt. 36, 8710–8723.
Richter, A., 2006. Differential optical absorption spectroscopy as a tool to measure pollution from space. Spectrosc. Eur. 18, 14–21.
Richter, A., Eisinger, M., Ladstätter-Weißenmayer, A., Burrows, J.P., 1999. DOAS zenith sky observations: 2. Seasonal variation of BrO over Bremen (53°N) 1994–1995. J. Atmos. Chem. 32, 83–99.
Richter, A., Eyring, V., Burrows, J.P., Bovensmann, H., Lauer, A., Sierk, B., Crutzen, P.J., 2004. Satellite measurements of NO_2 from international shipping emissions. Geophys. Res. Lett. 31, L23110. http://dx.doi.org/10.1029/2004GL020822.
Richter, A., Begoin, M., Hilboll, A., Burrows, J.P., 2011. An improved NO_2 retrieval for the GOME-2 satellite instrument. Atmos. Meas. Tech. 4, 1147–1159. http://dx.doi.org/10.5194/amt-4-1147-2011.
Rodgers, C.D., 2000. Inverse Methods for Atmospheric Sounding – Theory and Practice. In: Series on Atmospheric, Oceanic and Planetary Physics. World Scientific, Singapore.
Roscoe, H.K., Van Roozendael, M., Fayt, C., du Piesanie, A., Abuhassan, N., Adams, C., Akrami, M., Cede, A., Chong, J., Clémer, K., Friess, U., Gil Ojeda, M., Goutail, F., Graves, R., Griesfeller, A., Grossmann, K., Hemerijckx, G., Hendrick, F., Herman, J., Hermans, C., Irie, H., Johnston, P.V., Kanaya, Y., Kreher, K., Leigh, R., Merlaud, A., Mount, G.H., Navarro, M., Oetjen, H., Pazmino, A., Perez-Camacho, M., Peters, E., Pinardi, G., Puentedura, O., Richter, A., Schönhardt, A., Shaiganfar, R., Spinei, E., Strong, K., Takashima, H., Vlemmix, T., Vrekoussis, M., Wagner, T., Wittrock, F., Yela, M., Yilmaz, S., Boersma, F., Hains, J., Kroon, M., Piters, A., Kim, Y.J., 2010. Intercomparison of slant column measurements of NO_2 and O_4 by MAX-DOAS and zenith-sky UV and visible spectrometers. Atmos. Meas. Tech. 3, 1629–1646. http://dx.doi.org/10.5194/amt-3-1629-2010.
Rothman, L.S., Barbe, A., Benner, D.C., Brown, L.R., Camy-Peyret, C., Carleer, M.R., Chance, K., Clerbaux, C., Dana, V., Devi, V.M., Fayt, A., Flaud, J.-M., Gamache, R.R., Goldman, A., Jacquemart, D., Jucks, K.W., Lafferty, W.J., Mandin, J.-Y., Massie, S.T., Nemtchinov, V., Newnham, D.A., Perrin, A., Rinsland, C.P., Schroeder, J., Smith, K.M., Smith, M.A.H., Tang, K., Toth, R.A., Auwera, J.V., Varanasi, P., Yoshino, K., 2003. The HITRAN molecular spectroscopic database: edition of 2000 including updates through 2001. J. Quant. Spectrosc. Radiat. Transf. 82, 5–44.
Rozanov, A., Rozanov, V., Buchwitz, M., Kokhanovsky, A., Burrows, J.P., 2005. SCIATRAN 2.0 – a new radiative transfer model for geophysical applications in the 175–2400 nm spectral region. Adv. Space Res. 36, 1015–1019.
Sanders, R.W., 1993. Visible and near-ultraviolet spectroscopy at McMurdo Station, Antarctica 9. Observations of OClO from April to October 1991. J. Geophys. Res. 98, 7219–7228.
Serdyuchenko, A., Gorshelev, V., Weber, M., Chehade, W., Burrows, J.P., 2014. High spectral resolution ozone absorption cross-sections – part 2: temperature dependence. Atmos. Meas. Tech. 7, 625–636. http://dx.doi.org/10.5194/amt-7-625-2014.
Solomon, S., Schmeltekopf, A.L., Sanders, R.W., 1987. On the interpretation of zenith sky absorption measurements. J. Geophys. Res. 92, 8311–8319.
Takashima, H., Irie, H., Kanaya, Y., Syamsudin, F., 2012. NO_2 observations over the western Pacific and Indian Ocean by MAX-DOAS on Kaiyo, a Japanese research vessel. Atmos. Meas. Tech. 5, 2351–2360.
Vandaele, A.C., Hermans, C., Simon, P.C., Roozendael, M.V., Guilmot, J.M., Carleer, M., Colin, R., 1996. Fourier transform measurement of NO_2 absorption cross-section in the visible range at room temperature. J. Atmos. Chem. 25, 289–305.
Wagner, T., Dix, B., Friedeburg, C.V., Frieß, U., Sanghavi, S., Sinreich, R., Platt, U., 2004. MAX-DOAS O4 measurements: a new technique to derive information on atmospheric aerosols – principles and information content. J. Geophys. Res. D Atmos. 109, 1–19.
Wang, Y., Li, A., Xie, P.H., Wagner, T., Chen, H., Liu, W.Q., Liu, J.G., 2014. A rapid method to derive horizontal distributions of trace gases and aerosols near the surface using multi-axis differential optical absorption spectroscopy. Atmos. Meas. Tech. 7, 1663–1680. http://dx.doi.org/10.5194/amt-7-1663-2014.
Wittrock, F., 2006. The Retrieval of Oxygenated Volatile Organic Compounds by Remote Sensing Techniques. Ph.D.. University of Bremen, Bremen, Germany. Available at: http://www.doas-bremen.de/paper/diss_wittrock_06.pdf (last accessed May 2014).
Wittrock, F., Müller, R., Richter, A., Bovensmann, H., Burrows, J.P., 2000. Measurements of iodine monoxide (IO) above Spitsbergen. Geophys. Res. Lett. 27, 1471–1474.
Wittrock, F., Oetjen, H., Richter, A., Fietkau, S., Medeke, T., Rozanov, A., Burrows, J.P., 2004. MAX-DOAS measurements of atmospheric trace gases in Ny-Ålesund – radiative transfer studies and their application. Atmos. Chem. Phys. 4, 955–966. http://dx.doi.org/10.5194/acp-4-955-2004.